Experiments in Fluids 13, 63–70 (1992)

Experiments in Fluids

© Springer-Verlag 1992

Convection velocity measurements in a cylinder wake

Y. Zhou and **R. A. Antonia**

Dept. of Mechanical Engineering, University of Newcastle, N.S.W., 2308, Australia

Abstract. The convection velocity of vortices in the wake of a circular cylinder has been obtained by two different approaches. The first, implemented in a wind tunnel using an array of X-wires, consists in determining the velocity at the location of maximum spanwise vorticity. Four variants of the second method, which estimates the transit time of vortices tagged by heat or dye, were used in wind and water tunnels over a relatively large Reynolds number range. Results from the two methods are in good agreement with each other. Along the most probable vortex trajectory, there is only a small streamwise increase in the convection velocity for laminar conditions and a more substantial variation when the wake is turbulent. The convection velocity is generally greater than the local mean velocity and does not depend significantly on the Reynolds number.

Nomenclature

d	diameter of circular cylinder
f	frequency in spectrum analysis
f_v	average vortex frequency
r_v	vortex radius
Re	Reynolds number $\equiv U_0\, d/\nu$
t	time
Th_ω, Th_Γ, Th_r	thresholds for ω_{zp}, Γ, and r_v respectively
U_0	free stream velocity
U_1	maximum value of $(U_0-\bar{U})$
U_c	convection velocity of the vortex, as obtained either by Eq. (1) or Eq. (2)
U_{co}	convection velocity used in Eq. (3)
U_{cd}, U_{cu}	average convection velocities of downstream and upstream regions respectively of the vortex
U_{cv}	the value of U_c at $y=0.5\,\delta$
u, v	the velocity fluctuations in x and y directions respectively
$\bar{U}$, $\bar{V}$	mean velocity components in x and y directions respectively
U, V	$U=\bar{U}+u$, $V=\bar{V}+v$
x, y, z	co-ordinate axes, defined in Fig. 1

Greek Symbols

Γ	circulation
δ	mean velocity half-width
Δx	spacing between two cold wires or grid spacing
θ_1, θ_2	temperature signals from upstream and downstream cold wires respectively
ν	kinematic viscosity
τ_c	transit time for a vortex to travel a distance Δx
ϕ	phase in the cross-spectrum of θ_1 and θ_2
ω_z	instantaneous spanwise vorticity
ω_{zc}	cut-off vorticity used in determining the vortex size
ω_{zp}	peak value of ω_z
$\langle\rangle$	denotes conditional average, defined in Eq. (12)
$'$	prime denoting rms value

1 Introduction

Reliable estimates of U_c, the convection velocity of vortices shed from a circular cylinder, are important for several reasons. They are, for example, needed when it is necessary to view the flow field in a frame of reference which translates with the vortices (Cantwell and Coles 1983). They are also required for Taylor's hypothesis, i.e. for converting time derivatives into streamwise derivatives (e.g. Zaman and Hussain 1981).

Although previous measurements of U_c have been reported for the wake of a circular cylinder (e.g. Bloor and Gerrard 1966; Cantwell and Coles 1983; Hussain and Hayakawa 1987), there does not appear to have been a systematic study of the dependence of U_c on the distance from the cylinder, the Reynolds number or, more generally, the particular technique used for its determination. Also, the relationship between U_c and the local mean velocity $\bar{U}$ is not well established, although some investigators have assumed that U_c is equal to $\bar{U}$ in order to deduce the vortex path (Cantwell and Coles 1983).

In the present investigation, U_c and $\bar{U}$ were measured independently over relatively wide ranges of x/d and Re ($10 \le x/d \le 60$, $80 \le Re \le 13{,}700$). Two basically different approaches have been used to determine U_c. The first estimates the velocity at the maximum spanwise vorticity location. The second determines the transit time of heat- or dye-marked vortices. Four variants of the second method are considered. Flow visualizations of dye-marked vortices are briefly discussed in Section 4 in the context of previous work (e.g. Cimbala et al. 1988 and Hayakawa and Hussain 1989).

2 Experimental arrangements and conditions

2.1 Wind tunnel

(a) Details of the tunnel can be found in Browne and Antonia (1986). Three circular cylinders ($d=0.39$ mm, 2.60 mm and 12.50 mm) were used. Each cylinder was located in the mid-plane of the working section, 200 mm from the exit plane of the contraction, and spanned the width of the tunnel. The maximum blockage was 3.6%. The cylinders were slightly heated, the maximum average temperature rise (relative to the ambient free stream temperature) being no larger than 1.4 K in the region $x/d \geq 10$.

The two-cold-wire probe used for measuring U_c is sketched in Fig. 1. The Wollaston (Pt-10% Rh) wires (diameter = 1.27 μm, partly etched length $\simeq 1$ mm) were operated with constant current (0.1 mA) circuits. The separation Δx between the wires was 0.39 mm, 4.43 mm and 9.63 mm for $d=0.39$ mm, 2.60 mm and 12.50 mm, respectively. Signals from the circuits were offset, amplified and then digitized into a personal computer (NEC 386) (NEC, Tokyo, Japan) at a sampling frequency (20 to 50 kHz) sufficiently large to ensure adequate resolution of the time taken for a feature of the heat-marked vortex to travel a distance Δx. The duration of the digital records ranged from 10 to 15 s.

$\bar{U}$ was measured with a hot wire at the same x and y locations (but different z, see Fig. 1) as the two-cold-wire probe. The hot wire was calibrated in the free stream using a pitot static tube connected to a Baratron pressure transducer.

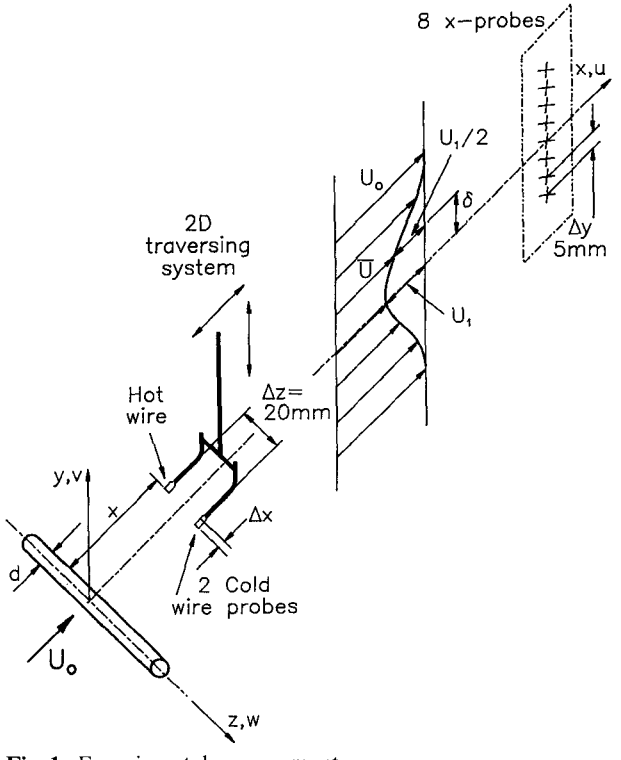

Fig. 1. Experimental arrangement

Measurements were made for $Re=80$, 470, 880, 1,450, 5,600 and 13,700 over the region $10 \leq x/d \leq 60$.

(b) In a separate topological investigation of the (x, y) plane, eight X-probes (Fig. 1) were used to provide measurements of u and v at eight y locations (Antonia 1991). The cylinder was not heated. In the present context, this arrangement is used to provide a relatively direct estimate of U_c at $Re=5{,}600$ and $10 \leq x/d \leq 60$.

The hot wires were similar to the one used in the heated wake. The signal from the circuits were offset, amplified, and digitized at a sampling frequency of 2,976 Hz. Using velocity and yaw calibrations, signals proportional to u and v were formed and stored on a magnetic tape (record duration $\simeq 30$ s).

Values of $\bar{U}$ and U_0 were obtained in a similar manner as for the heated wake.

2.2 Water tunnel

The water tunnel is a constant head recirculating two tank system. From a sump tank, a centrifugal pump (7.5 kW) delivers water to an annulus around the periphery of the head tank via a ring main. The combination of the ring main and annulus results in a relatively undisturbed flow into the contraction. A honeycomb is used to remove any large scale irregularities prior to the 3-D contraction (area ratio of approx. 6:1 over a height of 0.6 m), while the overflow from the head tank ensures a constant water head. The flow variation is controlled by an air-operated butterfly valve up to a maximum velocity, in the working section, of about 0.3 ms^{-1}.

The working section (260 mm × 260 mm × 2 m height) is made up of four 20 mm thick perspex panels. A cylinder ($d=4$ mm or 9.5 mm) was inserted at a distance of 120 mm from the working section entrance and spanned the full width of the tunnel. The resulting blockages were 1.5% ($d=4$ mm) and 3.7% ($d=9.5$ mm). Dye (diluted drawing ink) was introduced through an injection pinhole at the forward stagnation point of the cylinder. A high speed video camera (NAC, Osaka, Japan) was used to film the dyemarked vortex street at a rate of 400 frames per second. Illumination was provided by two strobes with a 1 μs flash rate. The photograph of one video frame is shown in Fig. 2. (The line that intersects the vortex street could not be avoided; it corresponds to the edge of the circular disc on which the cylinder was mounted). The grid (spacing $\Delta x=5$ mm), seen on the left side of Fig. 2, was superposed on the vortex street to provide a reference position for the vortices when estimating U_c. The number which can be seen on the grid is the value of x/d. When the video was played back, each frame was identified by a real time index (displayed on the top of Fig. 2), accurate to 2.5 ms. (The resulting maximum error in the transit time over a distance Δx is ± 2.5 ms).

A one-component (TSI, St. Paul, Minnesota, USA) laser Doppler anemometry system was used to measure $\bar{U}$ and U_0. The Doppler signal of velocity was processed by a model 1980B counter-type signal processor, and then digitized us-

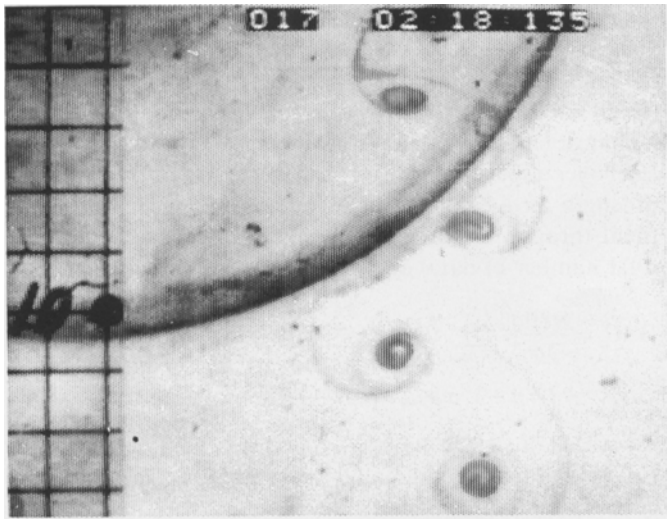

Fig. 2. Dye-marked vortices in near-wake ($Re=120$); the flow direction is top to bottom

ing a 4 channel, 12 bit AD converter into an NEC personal computer for analysis.

Flow visualization was carried out at $Re=120$ over the region $10 \leq x/d \leq 60$ and at $Re=290, 450$ for $x/d=10$ only (at large Re, the dye diffused too rapidly to be an effective marker of vortices for $x/d \geq 20$). $Re=450$ was selected to provide approximate overlap with one of the heated wake experiments ($Re=470$).

3 Description of methods

The convection velocity U_c has been obtained using two basic approaches:

I. by estimating the velocity at the vortex centre;
II. by determining the time τ_c taken by a characteristic feature of the vortex to travel a distance Δx, i.e.

$$U_c = \frac{\Delta x}{\tau_c}. \tag{1}$$

Method I is direct since vorticity, the main characteristic of the vortex, is identified. Method II is indirect since only characteristic features of the vortex – as marked, for example, by heat or dye – are identified. The effectiveness of this method depends on how well the vortex is marked. The marking is expected to become less effective as the distance from the cylinder increases. Several variants of Method II, labelled A–D in Table 1, were implemented. These variants, as well as Method I, are described below.

3.1 Method I

The value of U_c at location y is obtained by performing an ensemble average, viz.

$$U_c(y) = \frac{1}{n} \sum_{i=1}^{n} U_{ci}(y), \tag{2}$$

where $U_{ci}(y)$ is the velocity at the centre of the i^{th} vortex and n is the total number of vortices detected at the location y.

A detection scheme based on vorticity concentration, circulation and vortex size was used to identify vortices with respect to the time t and position y. Using instantaneous signals (U, V) formed by adding values of the local mean velocity $(\bar{U}, \bar{V})$ to the digital time series (u, v) of the velocity fluctuations, the instantaneous spanwise vorticity is approximated by

$$\omega_z = -\frac{\Delta V}{U_{co}\Delta t} - \frac{\Delta U}{\Delta y}, \tag{3}$$

where $\Delta y \approx 5$ mm is the spacing between X-probes and U_{co} is the convection velocity used for converting Δt into a streamwise separation. It was ascertained that the choice of U_{co} is not critical for determining peak vorticity locations. For example, at $x/d=10$, these locations were unaltered when U_{co} was varied between $0.85\ U_0$ and $0.95\ U_0$. The selected values of U_{co} (ranging from $0.85\ U_0$ to $0.91\ U_0$ as x/d increases from 10 to 60), are almost identical to those used by Hussain and Hayakawa (1987) or those obtained by Method II (Section 4).

Table 1. Summary of methods

Method	General description	Experimental facility	Vortex marker	Re	Number of detections	Estimates of uncertainty	Main sources of uncertainty
I	Vortex centre velocity	Wind tunnel	None	5,600	200 ~ 1,300 for each probe location	±2%	Velocity calibration and coarse lateral resolution ($\pm 0.2d$) in locating vortices
II	A. Conditional average B. Cross-correlation C. Phase	Wind tunnel	Heat	$80 \leq Re \leq 13{,}700$	2,000 ~ 4,000	±4%	Error in Δx, misalignment of cold and hot wires, time resolution (due to finite sampling frequency)
	D. Flow visualisation	Water tunnel	Dye	$120 \leq Re \leq 450$	30	±4%	Small size of the ensemble and time resolution (±2.5 ms)

One criterion used for detecting a vortex is

$$|\omega_{zp}| \geq Th_\omega , \tag{4}$$

where ω_{zp} is a peak value of vorticity and Th_ω is a threshold, at first chosen arbitrarily and later modified after examining the detected vortex locations on vorticity contour plots.

Two other criteria, involving the size and circulation of the vortex, were also applied. Before the size and circulation could be determined, an analytical expression for vorticity was required. A surface-fit technique, using a fifth-order Chebychev series, was applied to a rectangular grid (13 points in the x direction and 5 in the y direction), centred at the ω_{zp} location. An approximate analytical relation for ω_z was then established, i.e.

$$\omega_z = \omega_z(r, \alpha) , \tag{5}$$

where the origin of the cylindrical co-ordinate system was chosen at the location of ω_{zp}. To eliminate the angular parameter α in Eq. (5), ω_z is averaged with respect to α by

$$\bar{\omega}_z(r) = \frac{1}{2\pi} \int_0^{2\pi} \omega_z(r, \alpha)\, \mathrm{d}\alpha . \tag{6}$$

The vortex size is then estimated as the value of r_v for which

$$|\bar{\omega}_z(r_v)| = \omega_{zc} , \tag{7}$$

where ω_{zc} (≥ 0) is the assumed minimum vortex strength. While the choice of ω_{zc} clearly affects the value of r_v, it does not affect the vortex detection.

Once r_v is determined, the vortex circulation is calculated using

$$\Gamma = 2\pi \int_0^{r_c} \bar{\omega}_z(r)\, r\, \mathrm{d}r . \tag{8}$$

The magnitudes of Γ and r_v were required to satisfy the following conditions

$$|\Gamma| \geq Th_\Gamma \tag{9}$$

$$r_v \geq Th_r , \tag{10}$$

Th_Γ and Th_r being thresholds determined in similar fashion to Th_ω. In summary, the present vorticity detection criterion is based on the strength, circulation and size of the vortices, as represented by Eq. (4), (9) and (10), respectively.

The locations of the detected vortices were in excellent agreement with those observed from instantaneous vorticity contour plots. Also, the average number of detections at $x/d = 10$ indicated a vortex frequency of 0.203 U_0/d, a value within the expected range of $0.20 \sim 0.21\ U_0/d$ (Roshko 1954).

3.2 Method II

3.2.1 Conditional average

Characteristic features of heat-marked vortices (e.g. relatively sharp temperature increases and decreases associated with the downstream and upstream regions, respectively, of the vortex) were detected with the window average gradient (*WAG*) method described in detail in Antonia and Fulachier (1989) and Bisset et al. (1990). Briefly, this scheme identifies a change (either an increase or decrease) in average signal level over a specified time interval. A computational window of length $2\sigma+1$ points (digital samples) is moved point by point through the data $\theta(t_i)$ ($i = 1, 2, \ldots, N$, where N is the total number of data) and the value of WAG_j, where

$$WAG_j = \frac{\text{sign}}{2\sigma}\left(\sum_{i=j+1}^{j+\sigma} \theta(t_i) - \sum_{i=j-\sigma}^{j-1} \theta(t_i) \right), \tag{11}$$

$$j = \sigma+1, \sigma+2, \ldots, N-\sigma .$$

The value of *sign* is $+1$ or -1, and σ is set equal to about half the number of data points corresponding to the average vortex period.

A detection region begins when WAG_j first exceeds $k\theta'$ (k a threshold chosen such that the average detection frequency is approximately equal to the average vortex frequency) and ends when WAG_j drops below zero. The detection instant j_m within each detection region is the value of j for which WAG_j is largest. This occurs at the downstream and upstream regions when *sign* is $+1$ and -1, respectively.

The *WAG* technique was applied to $\theta_2(t_i)$, the temperature signal from downstream cold wire. Typical detections obtained for $sign = \pm 1$ are shown in Fig. 3. Averages of θ_2 and θ_1, conditioned on the *WAG* detections, were then obtained using

$$\langle \theta(\tau) \rangle = \frac{1}{n} \sum_{m=1}^{n} \theta(t_{jm} + \tau) , \tag{12}$$

where τ represents the time, relative to the detection instants t_{jm}, and n is the total number of detections. Examples of $\langle \theta_1 \rangle$ and $\langle \theta_2 \rangle$ are shown in Fig. 4. If $\tau = 0$ is the time at which the gradient of $\langle \theta_2 \rangle$ is maximum, τ_c can be identified with the time at which the gradient of $\langle \theta_1 \rangle$ is maximum. This is illustrated in Fig. 4a ($sign = +1$) and Fig. 4b ($sign = -1$).

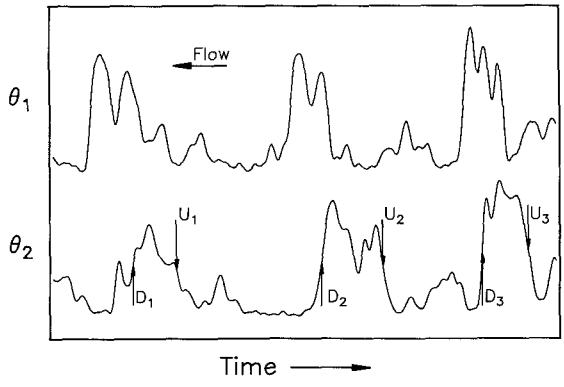

Fig. 3. Traces of θ_1 and θ_2 and detections using *WAG* technique (D_1, D_2 and D_3 denote downstream detections; U_1, U_2 and U_3 denote upstream detections); $Re = 5{,}600$, $x/d = 10$, $y/d = 0.96$, duration = 0.0256 s

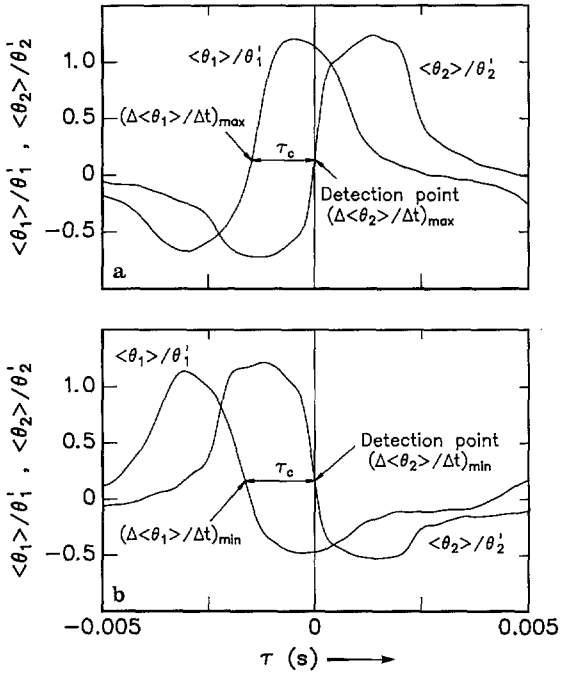

Fig. 4 a and b. Conditional averages $\langle\theta_1\rangle/\theta_1'$ and $\langle\theta_2\rangle/\theta_2'$; **a** *WAG* detections of downstream features of vortices; **b** *WAG* detections of upstream features of vortices

3.2.2 Correlation

The cross correlation $R_{\theta_1\theta_2}$ between θ_1 and θ_2 is defined by

$$R_{\theta_1\theta_2}(\tau)=\overline{\theta_1(t_i)\,\theta_2(t_i-\tau)}=\frac{1}{N}\sum_{i=1}^{N}\theta_1(t_i)\,\theta_2(t_i-\tau)\,, \qquad (13)$$

where τ is the time delay between θ_1 and θ_2. τ_c is identified with the time delay for which $R_{\theta_1\theta_2}$ is maximum.

3.2.3 Phase

The time τ_c is given by

$$\tau_c=\frac{\phi(f)}{2\pi f}\,, \qquad (14)$$

$\phi(f)$ being the phase $\tan^{-1} Q/Co$, where Q and Co are the quadrature spectrum and co-spectrum respectively of θ_1 and θ_2. In the range $x/d \lesssim 40$, f was taken equal to f_v, the average vortex frequency, which was clearly indicated by the location of the local maximum in the temperature spectrum. It was noted, however, that the ratio $\phi(f)/f$ was almost constant in the range $0<f\lesssim 2f_v$, so that the slope of the line of best fit to $\phi(f)$ vs $f\,(0<f\lesssim 2f_v)$ could also have been used to determine τ_c. This latter approach was followed for $x/d\gtrsim 40$, where the temperature spectrum did not exhibit a well defined maximum.

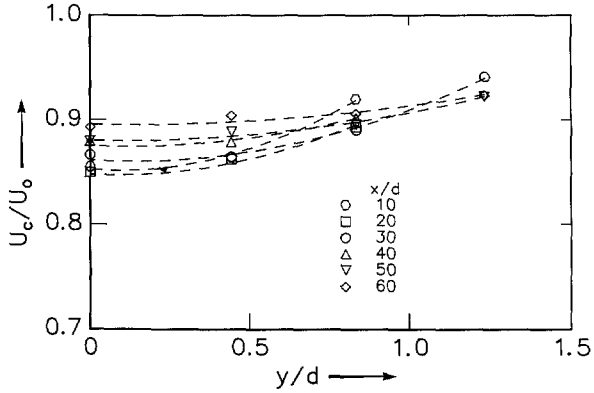

Fig. 5. Dependence of U_c on x/d and y/d; $Re=5{,}600$ (Method I); ○, $x/d=10$; □, 20; ○, 30; △, 40; ▽, 50; ◇, 60

3.2.4 Flow visualisation

On playing back the high speed video tape, τ_c was determined by identifying the instants of time at which chosen features, such as the leading or trailing edge of the dye concentration (e.g. Fig. 2), crossed the reference line on the grid (cf. Section 2). Note that the overall appearance and features of the dye-marked vortex street are very similar to those previously reported in the literature (e.g. Van Dyke 1982).

4 Results

Figure 5 shows the convection velocity obtained by Method I[1]. The symbols represent the values of U_c at the measurement locations, while the dashed lines are least square fits to these values. It is clear that at each x/d, U_c/U_0 increases with y/d. A similar behaviour is exhibited by the results from Methods IIA, IIB and IIC at six Reynolds numbers (only one example is shown in Fig. 7).

Figure 6 indicates that for Method IIA, the velocity U_{cd} of the downstream region of the vortex is greater than U_{cu}, the upstream velocity. The difference, consistent with a streamwise growth of the vortex, decreases as x/d increases and eventually vanishes for $x/d\geq 50$. The average of U_{cd} and U_{cu} was assigned to U_c, i.e.

$$U_c=\frac{(U_{cd}+U_{cu})}{2}\,. \qquad (15)$$

A typical distribution of U_c is shown in Fig. 7, the solid lines representing profiles of $\bar{U}$.

For Method IID, U_c was equal to the average value of the leading and trailing edge velocities of dye-marked vortices. It should, however, be noted that the leading and trailing edges of the dye may not always be in the same plane be-

[1] Results are presented for only one side of the wake centreline since the flow symmetry about the centreline was verified in both the present and previous experiments

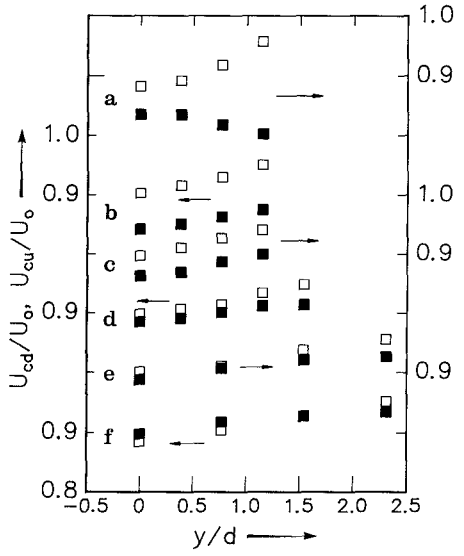

Fig. 6a–f. A comparison between U_{cu} and U_{cd} obtained by Method IIA; $Re = 880$; **a** $x/d = 10$; **b** 20; **c** 30; **d** 40; **e** 50; **f** 60; □, downstream; □, upstream ■

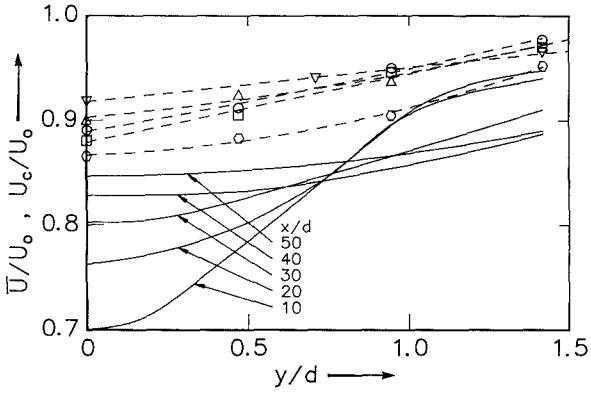

Fig. 7. Dependence of U_c/U_0 and $\bar{U}/U_0$ on x/d and y/d; $Re = 5{,}600$ (Method IIA); symbols are as in Fig. 5. —, $\frac{\bar{U}}{U_0}$

cause of the three-dimensionality of vortex rolls. These vortices were sometimes at a small inclination to the cylinder and remained tilted, occasionally becoming bent, as they travelled downstream. These are in agreement with previous observations based on flow visualisation and hot-wire measurements (Cimbala et al. 1988; Hayakawa and Hussain 1989). However, the streamwise vortices observed by Meiburg and Lasheras (1988) and Lasheras and Meiburg (1990) (both in flow visualisation and numerical simulations of a flat plate wake, $Re \approx 100$, subjected to initial periodic perturbations) were not seen clearly in the present visualisations. Although vortex pairing was observed ($x/d \approx 25$, $Re \simeq 250$), its frequency of occurrence was very small, implying that vortex pairing is unlikely to be responsible for the quasi-organised vortical motion in the far-wake.

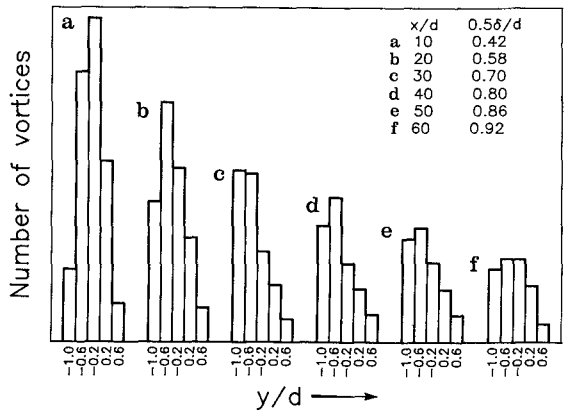

Fig. 8a–f. Histograms of detections (Method I)

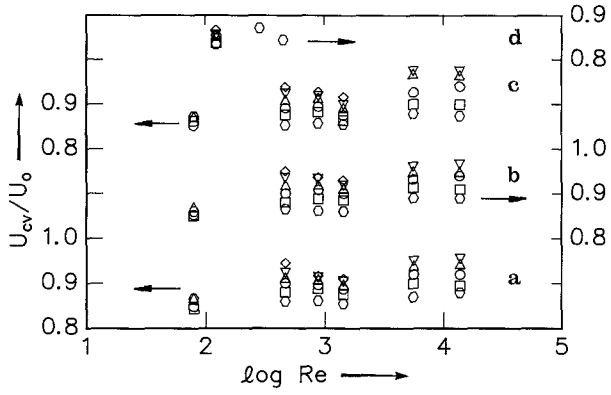

Fig. 9a–d. Dependence of U_{cv}/U_0 on Re and x/d; **a** Method IIA; **b** Method IIB; **c** Method IIC; **d** Method IID; symbols are as in Fig. 5

Since U_c/U_0 is not constant with respect to y/d, it is appropriate to give the value of U_c/U_0 at the most probable vortex location. Hussain and Hayakawa's (1987) results indicated that the locus of this location is given by $y_v \simeq 0.5\,\delta$ ($Re = 13{,}000$). Histograms of vortex locations, obtained by Method I, are shown in Fig. 8 for different x/d. For $x = 10d, 20d, 30d$ the histograms have peaks at $y = 0.4d$ ($\simeq 0.5\,\delta$), $0.6d$ ($\simeq 0.5\,\delta$), $0.8d$ ($\simeq 0.6\,\delta$), indicating good agreement with Hussain and Hayakawa's result. For $x/d \geq 40$, the vortices move further away from the centreline and a significant proportion of these vortices may not be captured by the present fixed array of X-probes. The result $y_v \simeq 0.5\,\delta$ is also supported by our flow visualisation observations (Method IID) at $Re = 120$. The measured average distances of the vortex centres from the centerline were $0.55d$ ($\simeq 0.4\,\delta$), $0.92d$ ($\simeq 0.5\,\delta$), $1.02d$ ($\simeq 0.6\,\delta$) at $x = 20d, 40d, 60d$, respectively. Assuming that $y_v = 0.5\,\delta$ is a reasonable approximation for the average vortex path, values of U_c (from Methods IIA, IIB, IIC and IID) at y_v, denoted by U_{cv}, have been plotted in Fig. 9. The results from Methods IIA, IIB, IIC compare favourably with those from Method IID for nearly overlapping Reynolds numbers.

Before discussing U_{cv}, an assessment of the effectiveness of heat as a passive marker of vortices is desirable. As noted previously, the basic difference between Methods I and II is that II focuses on a feature of the marked vortex, while in I, the velocity is determined at the vortex centre. It seems therefore reasonable to use I as reference for II in order to appraise the effectiveness of heat as a marker of the vortices. A comparison at the same Reynolds number ($Re=5{,}600$, Fig. 10) indicates that the two methods agree to within 3% at $x/d=10$. Since turbulence diffuses heat more easily than vorticity (e.g. Lesieur 1990), heat becomes a less effective marker as x/d increases, the vortex velocity tending to be slightly overestimated (by up to about 5%).

The behaviour of U_{cv} may be inferred from Figs. 9 and 10. For any particular value of x/d, U_{cv}/U_0 changes little with Re. The scatter in U_{cv}/U_0 increases for $x/d \geq 40$. This may be explained by the decreased effectiveness of heat as a vortex marker as x/d increases. It can also be seen that U_{cv}/U_0 changes with x/d. For laminar flow ($Re<160$), the variation is quite small, from about 0.84 to 0.87 in the range $10 \leq x/d \leq 60$. For turbulent flow, the variation is somewhat larger; U_{cv}/U_0 increases from 0.86 at $x/d=10$ to about 0.92 at $x/d=60$. These results compare favourably with previously reported values of U_c. For example, Karman and Rubach (see Goldstein 1965) indicated a value of 0.865 U_0 for Reynolds numbers up to 2,000 and Hussain and Hayakawa (1987) reported values in the range of 0.87 U_0 to 0.89 U_0 for $10 \leq x/d \leq 40$ at $Re=13{,}000$.

The value of U_{cv} is always greater than $\bar{U}$ (e.g. Fig. 7). At $x/d=10$, the ratio $(U_{cv}-\bar{U})/U_0$ (Fig. 11) is small in a laminar wake, but becomes significant in a turbulent wake. The difference between U_{cv} and $\bar{U}$ diminishes gradually as x/d increases and almost disappears for $x/d>40$.

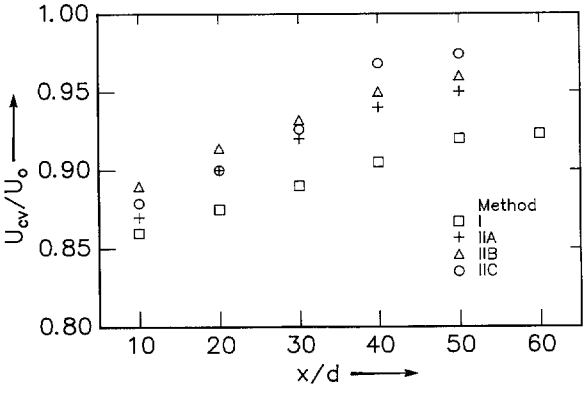

Fig. 10. Comparison between values of U_{cv}/U_0 obtained by the different methods; $Re=5{,}600$

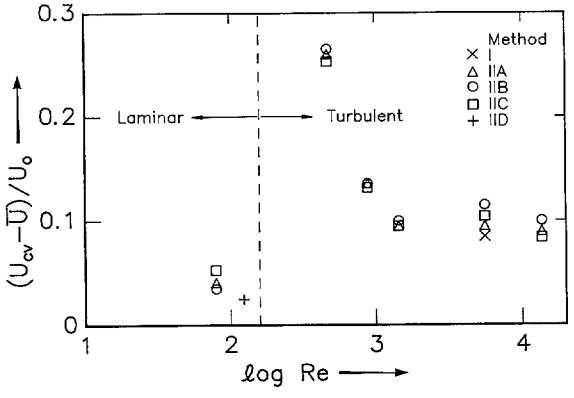

Fig. 11. Dependence of $(U_{cv}-\bar{U})/U_0$ on Re, $x/d=10$

5 Conclusions

The convection velocity of the wake vortices has been estimated using two basically different methods, including several variants of one of these methods. In all cases, consistent results are obtained:

1. The convection velocity increases with y/d and is generally larger than the local mean velocity. The difference between U_{cv} and $\bar{U}$ is small in a laminar wake but significant in a turbulent wake. This difference decreases with increasing x/d.
2. The ratio U_{cv}/U_0 is almost independent of the Reynolds number. In a laminar wake, its value is in the range 0.84 to 0.87 for $10 \leq x/d \leq 60$. In a turbulent wake, it increases slowly from about 0.86 at $x/d=10$ to 0.92 at $x/d=60$.
3. Heat, introduced at the cylinder, is a good marker of the vortices near the cylinder but becomes less effective at larger x/d. Although Methods IIA, B or C slightly overestimate the value of U_c, they are relatively easy to implement in wind tunnel.

References

Antonia, R. A. 1991: Organization in a turbulent near-wake. Fluid Dyn. Res. 7, 139–149

Antonia, R. A.; Fulachier, L. 1989: Topology of a turbulent boundary layer with and without wall suction. J. Fluid Mech. 198, 429–451

Bisset, D. K.; Antonia, R. A.; Browne, L. W. B. 1990: Spatial organization of large structures in the turbulent far-wake of a cylinder. J. Fluid Mech. 218, 439–461

Bloor, M. S.; Gerrard, J. H. 1966: Measurements on turbulent vortices in a cylinder wake. Proc. Royal Soc., Series A 294, 319–342

Browne, L. W. B.; Antonia, R. A. 1986: Reynolds shear stress and heat flux measurement in a cylinder wake. Phys. Fluids 29, 709–713

Cantwell, B.; Coles, D. 1983: An experimental study of entrainment and transport in the turbulent near wake of a circular cylinder. J. Fluid Mech. 136, 321–374

Cimbala, J. M.; Nagib, H. M.; Roshko, A. 1988: Large structure in the far wakes of two-dimensional bluff bodies. J. Fluid Mech. 190, 265–298

Goldstein, S. 1965: Modern developments in fluid dynamics, Vol. 2. Oxford: Clarendon Press

Hayakawa, M.; Hussain, F. 1989: Three-dimensionality of organized structures in a plane turbulent wake. J. Fluid Mech. 206, 375–404
Hussain, A. K. M. F.; Hayakawa, M. 1987: Eduction of large-scale organized structures in a turbulent plane wake. J. Fluid Mech. 180, 193–229
Lasheras, J. C.; Meiburg, E. 1990: Three dimensional vorticity modes in the wake of a flat plate. Phys. Fluids A 2, 371–380
Lesieur, M. 1990: Turbulence in fluids, p. 286. Dordrecht: Kluwer Academic
Meiburg, E.; Lasheras, J. C. 1988: Experimental and numerical investigation of the three-dimensional transition in plane wakes. J. Fluid Mech. 190, 1–37
Roshko, A. 1954: On the drag and shedding frequency of two-dimensional bluff bodies. Report NACA TN1191
Van Dyke, M. 1982: An album of fluid motion. Stanford: Parabolic Press
Zaman, K. B. M. Q.; Hussain, A. K. M. F. 1981: Taylor hypothesis and large-scale coherent structures. J. Fluid Mech. 112, 379–396

Received November 6, 1991

Technical notes

Visualization of roll-cell structure in turbulent wall jets along a strongly concave surface

N. Fujisawa

Dept. of Mechanical Engineering, Gunma University, Kiryu, 376 Japan

1 Introduction

Turbulent wall jets along a strongly concave surface have been investigated in relation to the production of Taylor-Görtler vortices by the centrifugal instability mechanism (Kobayashi and Fujisawa 1983). According to the linear stability analysis by Fujisawa and Shirai (1986), the concave turbulent wall jets become unstable against the centrifugal forces when the concave curvature parameter b/R exceeds 0.2, where b is the half width of the wall jet and R is the radius of the concave surface. In order to detect the Taylor-Görtler vortices experimentally, flow visualization studies were carried out for such a strong concave wall jet by the smoke-wire and tuft method (Fujisawa 1991). The visualized pictures indicate the presence of a roll-cell structure wandering randomly in space and time in a wide range of Reynolds numbers. Such an unsteady behavior of the vortices is similar to the observations by Barlow and Johnston (1988) in a natural turbulent boundary layer along a concave surface free of spanwise nonuniformity in the upstream condition.

The purpose of this note is to provide a better understanding of the roll-cell structure produced in the turbulent wall jets along a strongly concave surface, using an extensive smoke-wire visualization method with a moving laser-sheet illumination technique.

2 Experiments

The experimental arrangement for visualizing the flow structure of the turbulent wall jets along a strongly concave surface is shown in Fig. 1. An air jet issuing from the nozzle exit (height = 8 mm and width = 600 mm) develops on the leading flat plate of length $l_1 = 1{,}400$ mm to form a 2-D turbulent wall jet at the start of the concave section. The concave plate is made of a transparent polycarbonate with a constant concave radius $R = 250$ mm. This plate is also used for the visualization study of plane wall jets by stretching it flat. The wall jet is turned at right angle by the concave section and flows along the following flat plate of length $l_2 = 400$ mm. This flow configuration is the same as in the flow measurement by Kobayashi and Fujisawa (1983), and hence the curvature parameter b/R at the start of the concave section is expected to be about 0.45, which satisfies the theoretical

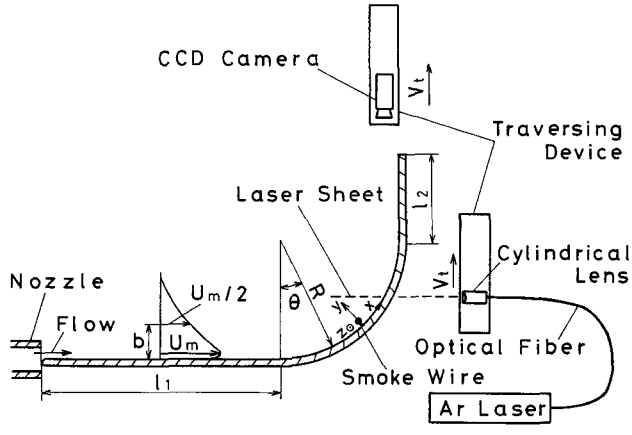

Fig. 1. Schematic diagram of experimental apparatus ($R = 250$ mm, $l_1 = 1{,}400$ mm, $l_2 = 400$ mm)